

Article

Facile Elaboration of Wet Cellulose Film as Catalyst Support of MnO_x Nanoparticles for the Catalytic Oxidation of Dyes in Absence of Light

Larissa V. F. Oliveira ^{1,2,3}, Lionel Limousy ^{1,2,*}, Simona Bennici ^{1,2,*}, Ludovic Josien ^{1,2}, Samar Hajjar-Garreau ^{1,2}, Mary-Lorène Goddard ^{4,5,6}, Marcos A. Bizeto ³ and Fernanda F. Camilo ³

¹ CNRS, IS2M UMR 7361, Université de Haute-Alsace, F-68100 Mulhouse, France; larissavfoliveira@hotmail.com (L.V.F.O.); ludovic.josien@uha.fr (L.J.); samar.hajjar@uha.fr (S.H.-G.)

² CNRS, UMR 7361, Université de Strasbourg, 67000 Strasbourg, France

³ Laboratório de Materiais Híbridos, Departamento de Química, Instituto de Ciências Ambientais, Químicas e Farmacêuticas, Universidade Federal de São Paulo, Campus Diadema, São Paulo 18052-780, Brazil; mabizeto@unifesp.br (M.A.B.); ffcamilo@unifesp.br (F.F.C.)

⁴ Laboratoire d'Innovation Moléculaire et Applications UMR CNRS 7042-LIMA, Université de Haute-Alsace, 3bis rue Alfred Werner, CEDEX 68093 Mulhouse, France; mary-lorene.goddard@uha.fr

⁵ Laboratoire d'Innovation Moléculaire et Applications UMR CNRS 7042-LIMA, Université de Strasbourg, 3bis rue Alfred Werner, CEDEX 68093 Mulhouse, France

⁶ Laboratoire Vigne, Biotechnologies et Environnement EA 3991, Université de Haute-Alsace, 33 rue de Herrlisheim, 68008 Colmar, France

* Correspondence: lionel.limousy@uha.fr (L.L.); simona.bennici@uha.fr (S.B.); Tel.: +33-3-89608705 (L.L.); +33-3-893-36729 (S.B.)



Citation: Oliveira, L.V.F.; Limousy, L.; Bennici, S.; Josien, L.; Hajjar-Garreau, S.; Goddard, M.-L.; Bizeto, M.A.; Camilo, F.F. Facile Elaboration of Wet Cellulose Film as Catalyst Support of MnO_x Nanoparticles for the Catalytic Oxidation of Dyes in Absence of Light. *Clean Technol.* **2021**, *3*, 288–298. <https://doi.org/10.3390/cleantechnol3020016>

Academic Editor: Raffaele Marotta

Received: 17 January 2021

Accepted: 19 March 2021

Published: 31 March 2021

Publisher's Note: MDPI stays neutral with regard to jurisdictional claims in published maps and institutional affiliations.



Copyright: © 2021 by the authors. Licensee MDPI, Basel, Switzerland. This article is an open access article distributed under the terms and conditions of the Creative Commons Attribution (CC BY) license (<https://creativecommons.org/licenses/by/4.0/>).

Abstract: In the present work a remarkably simple procedure for the elaboration of wet cellulose film containing manganese oxide nanoparticles was developed. The films were produced using a mold made by 3D printing using cellulose dissolved in an ionic liquid, which allows the production of thin and homogeneous films of different shapes, types and designs which cannot be made using conventional techniques. Thanks to this possibility, the final catalytic object can be implemented in specific reactors. Manganese oxide nanoparticles were prepared as a colloidal solution by a redox/sol-gel procedure and then deposited on the cellulose films by wet impregnation. The catalytic film obtained was tested in the decomposition of a dye, indigo carmine (IC), in the absence of light. The influence of the pH of the solution on the decomposition rate was investigated. IC total decomposition was measured after 1-h reaction at pH below 3. At pH = 2, no deactivation of the catalyst was observed even after four decomposition cycles. This work provides a new strategy to design cellulose-based catalysts for dye removal from wastewater.

Keywords: cellulose film; MnO_x nanoparticles; catalytic oxidation; indigo carmine dye

1. Introduction

The presence of dyes in wastewater represents a worldwide environmental issue and many solutions have been proposed to eliminate these polluting compounds [1]. Unfortunately, the non-selectivity and the high operational costs of the studied systems still represent a drawback to their extensive implementation [2,3]. A promising approach to limit the operational cost of dyes removal is the elaboration of new oxidation catalysts containing manganese oxide nanoparticles [4,5]. Manganese oxide is cheap, chemically stable, and not toxic for the environment. Focusing on the catalytic application, the use of manganese oxide nanoparticles in powder or in dispersion has some obstacles, due to the aggregation and/or agglomeration during the use, which leads to the loss of the catalytic activity [6,7]. To overcome this impasse, these nanoparticles can be supported in different substrates, such as polymeric membranes [8]. Most of the polymeric matrixes used to this end are obtained from petrochemical sources and they are non-degradable, persisting

in nature for many years. Considering the recent concerns on environmental issues, the interest in using polymeric materials originated from renewable sources is emerging. Among these materials, cellulose has great potential to fulfill those requirements due to its low cost, abundance, renewability and biodegradability [9]. Nonetheless, cellulose has poor solubility and processability, disadvantages which have been overcome when specific ionic liquids were capable to dissolve this biomass [10] and to produce cellulose films by the regeneration of the dissolved cellulose with an anti-solvent [11]. The search for catalyst based on non-modified cellulose and manganese oxides are still scarce and recent. In 2019, Peng and co-workers [12] produced porous cellulose film containing MnO₂ microspheres spread in the reticular structure of the biopolymer. The film efficiently degraded acid orange in wastewater. In our previous study, we produced free-standing films of non-modified cellulose impregnated with manganese dioxide nanoparticles and their application in the discoloration of the indigo carmine dye upon exposure to ambient light [13].

In the present work, a new approach to produce supported MnO_x nanoparticles on wet cellulose films with controlled shape and thickness is described. The films were produced using a mold made by 3D printing, which allows the production of thin and homogeneous films of different shapes, types and designs which cannot be made using conventional techniques. X-ray Photoelectron Spectroscopy (XPS) measurements of this film was fundamental to evaluate the interaction between the biopolymer and the metal oxide. XPS analyses involving cellulose films are scarce in the literature. The cellulose support is cheap, easy to prepare, biodegradable, abundant, non-toxic and allows to obtain new nanocatalysts [13–17]. The discoloration of indigo carmine was evaluated in the absence of light, proving that this film does not act as photocatalytic.

2. Materials and Methods

The active phase (MnO_x-nanoparticles) was prepared starting from tetramethylammonium permanganate (TMAMnO₄) synthesized following the same protocol used by Brock et al. [18]. A deionized water solution (10 mL) containing 2.54 g of tetramethylammonium bromide dissolved in 25 mL of deionized water was added dropwise to a water solution containing 2.37 g of KMnO₄ under stirring for 1 h at room temperature. The TMAMnO₄ precipitated was then recovered by filtration and dried. The preparation of manganese dioxide nanoparticles suspension was carried out by dissolving 290 mg of TMAMnO₄ in a mixture constituted of 30.0 mL of 2-butanol and 30.0 mL of deionized water, at room temperature and under stirring for 1 h. The organic and aqueous phases were separated. MnO_x suspension was obtained in the aqueous phase. This sample was labelled "MnO_x_suspension". Then, the suspension containing manganese oxide nanoparticles was ready to be deposited onto the cellulose film.

In order to prepare the cellulose film, firstly, microcrystalline cellulose was dissolved in an ionic liquid (1-butyl-3-methylimidazolium chloride-BMImCl) at 60 °C for 24 h. The obtained solution (5.0 wt%) was highly viscous and needed to be maintained at 60 °C to avoid solidification. A specific mold and spatula (both made of polycarbonate) were purposely produced using a 3D printing system in order to obtain the wanted shape of cellulose film used as catalytic support (Figure 1a). First, a sufficient amount of the cellulose solution was deposited at the extremity of the mold (Figure 1b) and spread with the spatula with a slow and continuous movement in order to cover all the surface of the mold, thus avoiding the formation of holes or air bubbles. The space between the spatula and the surface of the mold was equal to 1 mm. To regenerate the dissolved cellulose as a film, distilled water was added (Figure 1c). The resulting film (Figure 1d) was rinsed with distilled water to remove all the ionic liquid. The complete removal of BMImCl was checked by collecting drops from the washing water and adding drops of 0.1 M aqueous solution of silver nitrate. The membrane is free of chloride if the solution remains clear in this test after the addition of silver nitrate. The complete removal of the ionic liquid is crucial to prevent the agglomeration of the MnO_x nanoparticles in the next step. Finally,

the MnO_x suspension was left in contact with the film during 12 h. Then, the film was washed with distilled water exhaustively (Figure 1e) and stored in distilled water before use. These samples are denominated as Cellulose_MnO_x (CEL_MnO_x). The obtained films presented a homogenous thickness of 1 mm, a width of 35 mm and a length of 250 mm. The walls of the mold were dimensioned to accept, without overflowing, 20 mL of the MnO_x suspension. Eight round shaped films (diameter = 2.0 cm; average area = 6.2 cm² considering both sides) were produced.

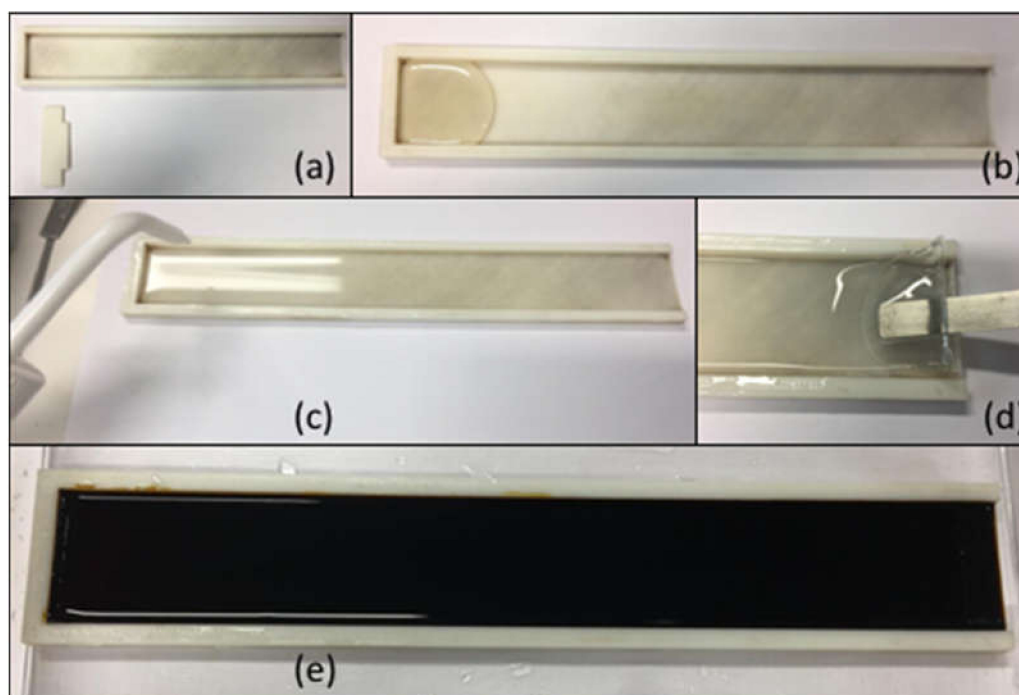


Figure 1. Description of the different steps necessary to produce the wet cellulose film containing MnO_x nanoparticles: (a) mold and spatula; (b) deposit of the cellulose solution; (c) extraction of the ionic liquid with distilled water; (d) stripping of the wet cellulose film; (e) cellulose film in contact with the MnO_x suspension.

The isoelectric point of the MnO_x-nanoparticles was measured by Zeta potential measurements at different pH. To perform these experiments, the aqueous suspension containing 0.05 mol L⁻¹ of MnO₂ nanoparticles was recovered in powder form after water removal. This sample was labelled “MnO_x_powder”. Eight suspensions containing 40 mg of the MnO_x_powder sample and 50 mL of an aqueous solution of NaCl (0.001 M) were prepared with pH in the 2–8 range. The pH was adjusted by adding HCl or NaOH solutions (0.1 M). Each sample was maintained under stirring for 24 h. The pH of the suspensions was measured before and after the 24 h stirring. In case of variation of the pH, HCl or NaOH solutions were added again. The resulting suspension was then maintained under stirring for 24 supplementary hours. This procedure was repeated until stabilization of the pH. The measurements were taken after pH stabilization. The Zeta potential values were obtained using a Malvern Zetasizer. Five zeta measurements were performed for each suspension of MnO_x-nanoparticles at different pH.

The diffusion light scattering (DLS) measurements of the MnO_x suspension were obtained also using a Malvern Zetasizer. The suspensions used for these measurements were the same than elaborated for zeta potential measurements.

X-ray photoelectron spectroscopy (XPS) measurements were carried out on a VG Scienta SES 2002 spectrometer (Uppsala, Sweden) equipped with a monochromatic Al K α X-ray source (Al K α = 1486.6 eV) and a hemispherical analyzer (Uppsala, Sweden).

Scanning transmission electron microscopy (STEM) images were obtained with a JSM-7900 JEOL microscope equipped with a Deben STEM detector, at an accelerating voltage of 30 kV.

The catalytic properties were tested by immersing the round film in 10 mL indigo carmine aqueous solution (20 ppm) for 1 h at different pH-values. The pH was adjusted by addition of HCl solution (1.0 M). All the experiments were carried out in absence of light. The indigo carmine degradation was monitored spectrophotometrically following the intensity of the band at 610 nm. All the experiments were carried out with fresh pieces of the catalyst (coming from the same cellulosic film), except the experiments corresponding to the cycling tests. For this last, the catalyst was rinsed with deionized water until no indigo carmine (IC) dye is present.

The color removal efficiency of the dye was estimated through Equation (1):

$$\% \text{Color removal} = \frac{(C_i - C_t) * 100}{C_i} \quad (1)$$

C_i and C_t are the concentration of IC at time zero and time t , respectively.

The Langmuir-Hinshelwood (L-H) model [19] was used to describe the degradation reaction of IC occurring at the solid-liquid interface between the cellulosic film and the IC solution. The degradation rate (τ) of IC can be estimated through Equation (2):

$$\tau = -\frac{d[\text{IC}]}{dt} = \frac{k_r K [\text{IC}]_0}{1 + K [\text{IC}]_0} \quad (2)$$

where $[\text{IC}]_0$ (ppm or mg L^{-1}) is the initial concentration of indigo carmine, k_r (min^{-1}) is the reaction rate constant at maximum surface coverage, and K (dimensionless) is the equilibrium adsorption coefficient.

Considering that $[\text{IC}]_0$ is very small, after integration and rearrangement, Equation (2) becomes Equation (3):

$$\ln \frac{[\text{IC}]_0}{[\text{IC}]} = k_r K t = k' t \quad (3)$$

where k' corresponds to the apparent constant rate of IC degradation.

3. Results and Discussion

3.1. Film Characterization

Five zeta-measurements were performed for each suspension of MnO_x -nanoparticles at different pH. Then, the mean and standard deviation of the values were obtained. The isoelectric point (IEP) of the MnO_x nanoparticles was estimated plotting the zeta potential curve (Figure 2). The IEP for the MnO_x nanoparticles was evaluated around $\text{pH} = 4$. This means that the surface of the particles is positively charged for pH lower than 4 (blue square) and negatively charged at higher pH values. This result is consistent with the values found in the literature, which show a pH_{pzc} between 3.3 and 4 for δ and β - MnO_2 nanoparticles [20,21].

STEM characterizations and diffusion light scattering (DLS) analysis were done in order to estimate the particle size distribution of the MnO_x nanoparticles. Figure 3 shows the distribution of the MnO_x nanoparticles in the cellulose film. Particles with a mean diameter in the 80–100 nm range were observed (Figure 3b). At a higher magnification (Figure 3c), it was possible to observe that the nanoparticles correspond to an agglomeration of smaller ones. This result was confirmed by DLS measurements (not reported here) that show a bimodal dispersion with average diameters around 10 and 80 nm. The particles with diameter of 80 nm correspond to the agglomeration of smaller nanoparticles.

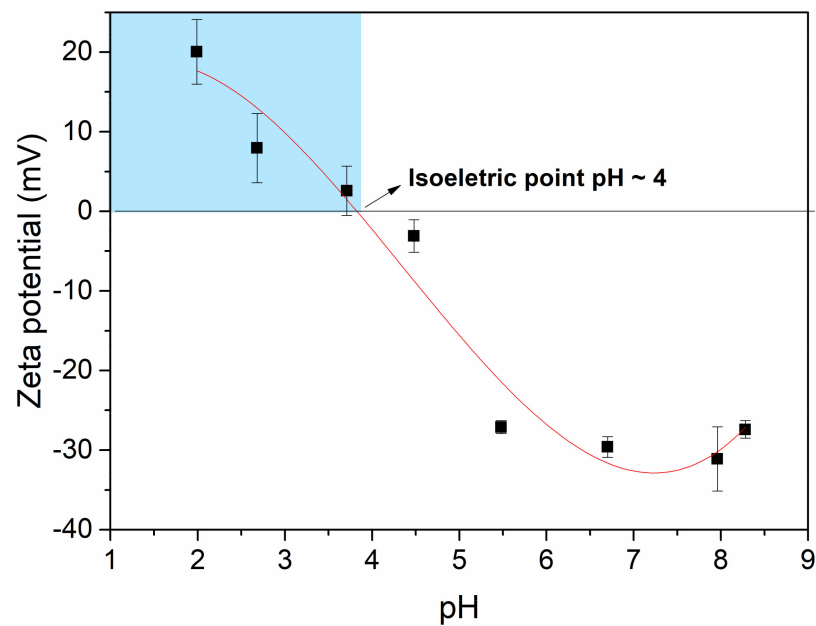


Figure 2. Zeta potential measurements carried out on the MnO_x nanoparticles suspensions obtained in different pH. A third-degree polynomial (red curve) fits the data.

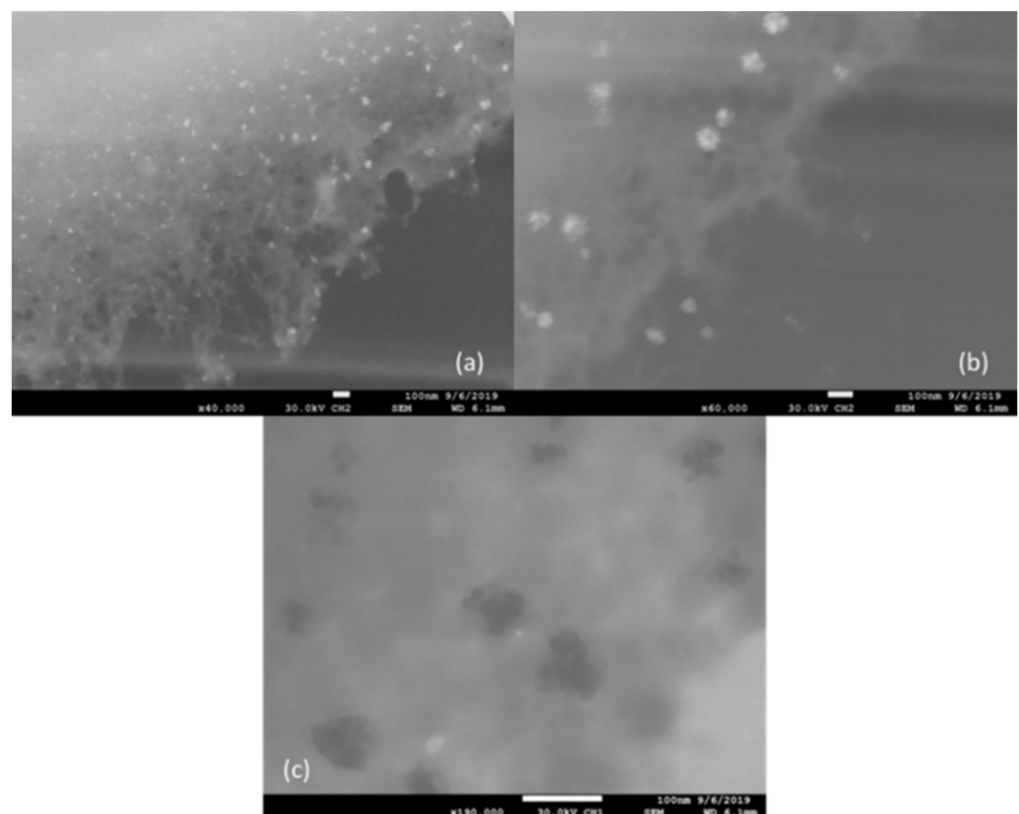


Figure 3. STEM images obtained at different magnifications on the cellulose film containing MnO_x nanoparticles: (a) $\times 40,000$; (b) $\times 60,000$; (c) $\times 190,000$.

XPS analysis was carried out to determine the redox state of Mn (Figure 4). All data acquired on the cellulose film containing MnO_x and pure cellulose film are reported in detail in Tables 1 and 2, respectively. The survey spectrum of the CEL_MnO_x sample (Figure 4a) shows the major presence of O, C, Mn and, at a lower extent, N and Si. Si corresponds to an impurity of the microcrystalline cellulose, while N derives from the

residual ionic liquid. The Mn content was estimated at 9 wt%. Mn 2p spectrum (Figure 4b) displays two contributions, located around 642.4 eV and 654.2 eV, attributed respectively to Mn2p_{3/2} and Mn2p_{1/2}, and with a spin-orbit coupling of 11.8 eV. This spectrum exhibits a multiplet splitting that was fitted in accordance with reference [22]. The deconvolution of this peak confirms the presence of MnO₂ and enables to estimate the Mn IV and Mn III amounts, 88.5 at% for Mn IV (MnO₂) and 11.5 at% for Mn III, respectively. The presence of covalent C-O-Mn bonds was enlightened by analyzing the C1s and O1s XPS spectra of the cellulose film before (Figure 5b,c) and after (Figure 4c,d) the deposition of MnO_x-nanoparticles. The C1s presented different contributions respectively assigned to C-C and C-H (285 eV), C_a (286.7 eV), and C_b (288.3 eV). The O1s peak was deconvoluted in two picks: O_a (532.7 eV) and O_b (533.3 eV). The C_a and C_b contributions describe the carbon-oxygen bond in C-OR, R=H or C or Mn species. The components O_a and O_b come only from bonds between carbon and oxygen (C-OR, R=H or C). A third O1s contribution corresponding to O₂- (MnO₂) and Mn-O-C bonds was detected only in the CEL_MnO_x sample.

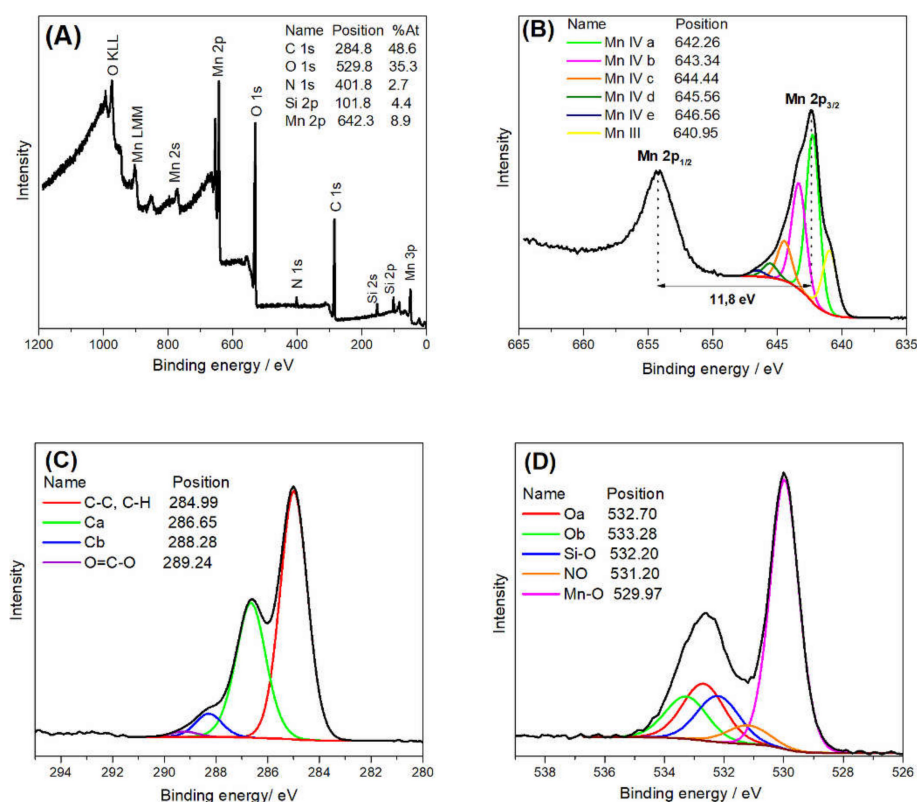


Figure 4. XPS spectra of the cellulose film containing MnO_x nanoparticles. (A) Survey spectrum; (B) Mn 2p; (C) C 1s; (D) O 1s.

The deconvolution of the C1s and O1s peaks allowed calculation of the concentration (%At) of each contribution (see Table 2). The $(C_a + C_b)/(O_a + O_b)$ ratio for the bare cellulose film (equal to 1.35) was supposed not to vary in the film containing MnO_x if no new carbon-oxygen bonds were formed. However, the ratio value increased to 1.9 indicating the presence of a new interaction between cellulose and manganese oxide (lower $O_a + O_b$ value). This indicates that some C-O-H bonds transform into C-O-Mn, and that the MnO_x nanoparticles are strongly bonded to the cellulose matrix.

3.2. Catalytic Oxidation of Indigo Carmine Dye

We compared the degradation of IC in dark and under light condition. The results showed that light has no impact on the reaction; in other words, in dark condition the degradation rate is the same that of under light condition. This shows that the degradation

of IC by this film is not a photocatalytic reaction but a chemical catalysis reaction. In front of this result, all catalyst tests were performed in the absence of light.

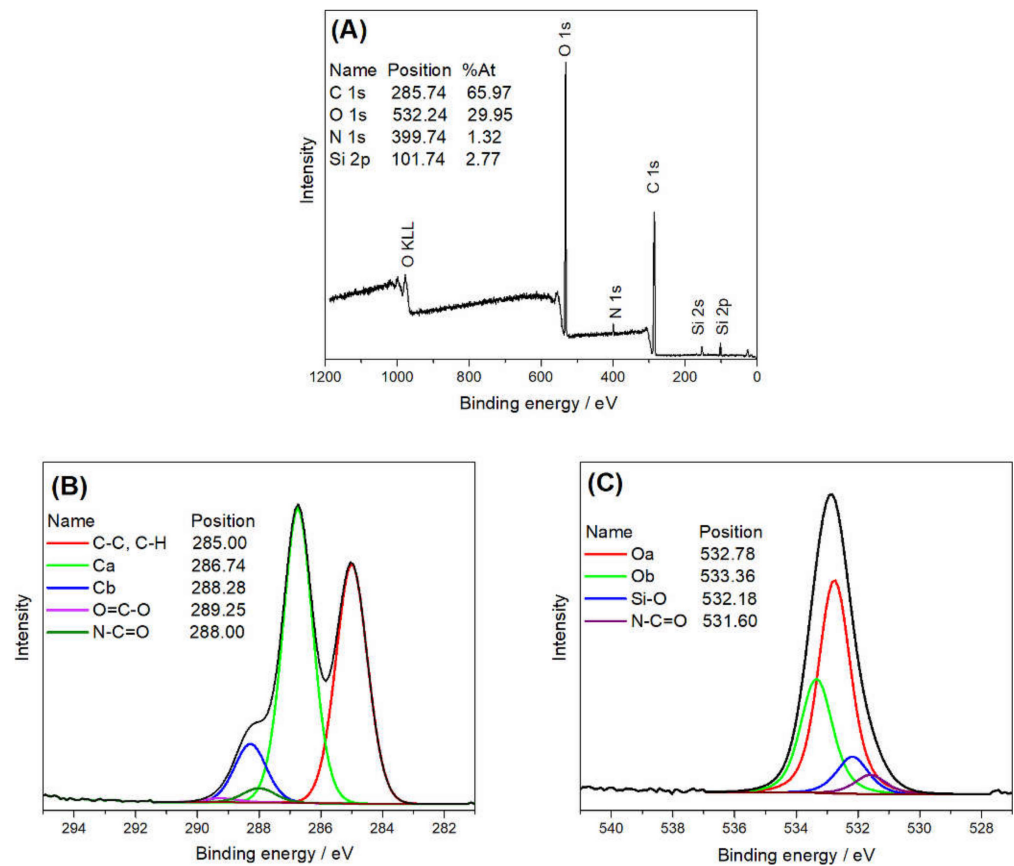


Figure 5. XPS spectra of the bare cellulose film. (A) Survey spectrum; (B) C 1s; (C) O 1s.

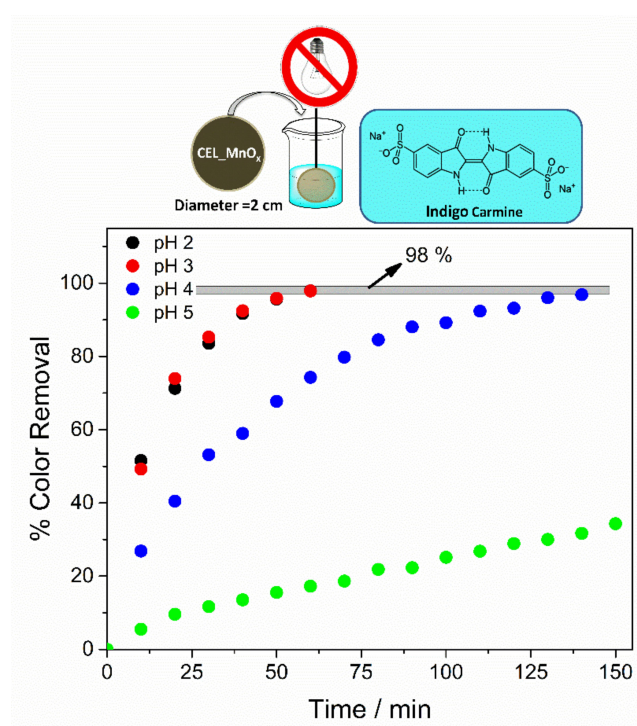
Table 1. XPS data for the cellulose film containing MnO_x nanoparticles.

Spectrum	Attribution	Binding Energy ± 0.1 (eV)	Atomic Concentration ± 0.05 (%)
C 1s	Ca	286.65	16.77
C 1s	Cb	288.28	2.53
O 1s	Oa	532.70	5.85
O 1s	Ob	533.28	4.37
O 1s	Si-O	532.20	4.66
O 1s	Mn-O	529.97	19.24
O 1s	NO	531.20	1.92
C 1s	C-C C-H	284.99	27.83
C 1s	O=C-O	289.24	0.57
N 1s	C-N	400.00	0.79
N 1s	NO	402.39	1.92
Si 2p	Si 2p _{3/2} Si(-O) ₂	102.22	4.66
Mn 2p	Mn a (Mn IV)	642.26	3.79
Mn 2p	Mn b (Mn IV)	643.34	2.59
Mn 2p	Mn c (Mn IV)	644.44	0.98
Mn2p	Mn d (Mn IV)	645.56	0.35
Mn2p	Mn e (Mn IV)	646.56	0.16
Mn2p	Mn III	640.95	1.02

Table 2. XPS data for the bare cellulose film.

Spectrum	Attribution	Binding Energy ± 0.1 (eV)	Atomic Concentration ± 0.05 (%)
C 1s	Ca	286.74	30.02
C 1s	Cb	288.28	6.33
O 1s	Oa	532.78	17.59
O 1s	Ob	533.36	9.4
O 1s	Si-O	532.2	2.97
O 1s	N-C=O	531.6	1.53
C 1s	C-C, C-H	285	25.61
C 1s	O=C-O	289.25	0.44
C 1s	O=C-N	288	1.54
N 1s	C-N	400.15	1.58
Si 2p	Si 2p _{3/2} Si(-O) ₂	102.18	2.98

The dye discoloration results performed in different pH are presented in Figure 6. The used pH values were selected in order to correlate the isoelectric point values of the MnO_x nanoparticles to the discoloration performances. At pH lower than 3, the color removal reached a maximum of 98% at a reaction time of 60 min, increasing to 150 min when pH = 4 was used. No appreciable discoloration was observed in pH higher than 5 even after 150 min. The IEP for the MnO_x nanoparticles was evaluated around pH = 4 (see Section 3.1). The surface of the particles was then positively charged for pH lower than 4 and negatively charged at higher pH values. As indigo carmine is an anionic dye, repulsion between the dye and the MnO_x nanoparticles may occur at pH higher than 4, limiting the catalytic process. Considering only the first 60 min, a linear relationship between $\ln \frac{[IC]_0}{[IC]}$ versus time, as shown in Figure 7 indicated that the reaction was first order with respect to IC. The apparent rate constant was calculated from the slope of the plot of $\ln \frac{[IC]_0}{[IC]}$ versus time. k_{app} values (inset in Figure 7) were close to each other in pH 2 and 3 as expected and decreased markedly at pH = 5 due to the absence of interaction between the catalyst and the dye.

**Figure 6.** Scheme of the discoloration test and graph of the color removal (%) vs. time at different pH values.

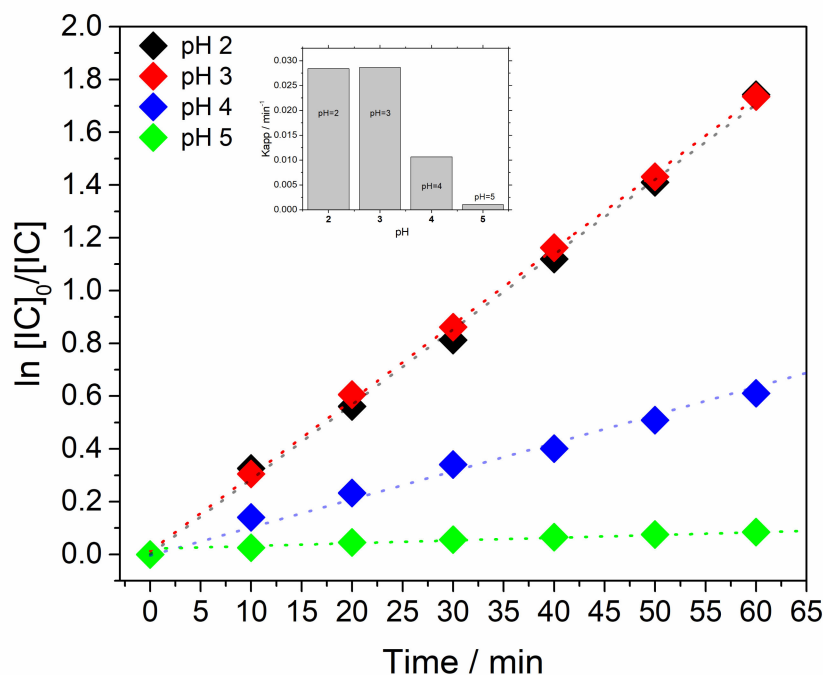


Figure 7. Kinetics of indigo carmine (IC) degradation according to the pH of the solution represented through the Langmuir-Hinshelwood (L-H) model. Inset: k_{app} values.

The cellulose film containing MnO_x nanoparticles passed for the reusability catalytic test (Figure 8). In these experiments, after 60 min, the film was removed from reaction media using a tweezer. Four cycles were evaluated, and samples were collected every 10 min. Promisingly, no deactivation of the catalyst was measured after performing four degradation cycles at pH = 2 during 1 h; the discoloration was maintained higher than 95%. The k_{app} values are practically maintained in the four consecutive reaction cycles (inset Figure 8).

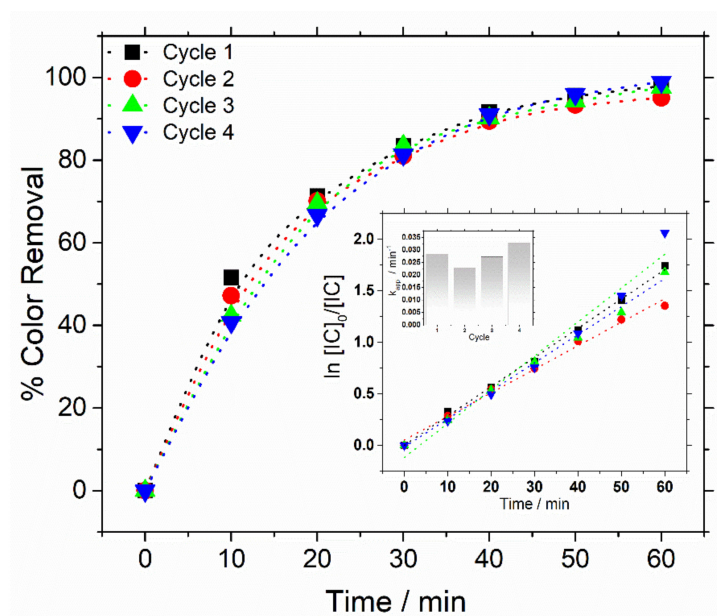


Figure 8. Reusability catalytic test using the same cellulose film containing MnO_x nanoparticles.

4. Conclusions

Dissolved cellulose can be spread in different molds made by 3D printing, which allows the production of films with different shapes, thicknesses and designs, opening the possibility to be implemented in specific reactors.

A new catalyst constituted of a cellulose film impregnated with MnO_x nanoparticles was produced in the present work. The characterizations showed that the active phase particles are constituted of an agglomeration of MnO_x nanoparticles, mainly present as MnO₂. Covalent bonding was detected between the cellulose support and the nanoparticles, which leads to a good stability of the nanocatalyst. The catalytic properties were evaluated for the indigo carmine discoloration in absence of light at different pHs. The results show that the oxidation of the dye reaches the maximum at pH lower than 3. The catalytic activity remained constant after four cycles of degradation. These promising results enable a new approach for the facile elaboration of low-cost, non-toxic and biodegradable catalysts based on cellulose.

Author Contributions: Conceptualization, L.L. and F.F.C.; methodology, L.L.; validation, L.L. and S.B.; formal analysis, L.V.F.O. and S.B.; investigation, L.V.F.O., L.J., and S.H.-G.; resources, M.A.B., L.L., S.B. and F.F.C.; data curation, L.L., S.B. and L.V.F.O.; writing—original draft preparation, L.V.F.O.; writing—review and editing, S.B. and L.L.; supervision, L.L., F.F.C., M.A.B. and M.-L.G.; funding acquisition, F.F.C. All authors have read and agreed to the published version of the manuscript.

Funding: This research was funded in part by the Coordenação de Aperfeiçoamento de Pessoal de Nível Superior—Brasil (CAPES)—Finance Code 001. The authors gratefully acknowledge the financial support from Fundação de Amparo à Pesquisa do Estado de São Paulo (FAPESP, grant number 2018/20826-4).

Institutional Review Board Statement: Not applicable.

Informed Consent Statement: Not applicable.

Data Availability Statement: The datasets generated during and/or analysed during the current study are available from the corresponding authors on reasonable request.

Conflicts of Interest: The authors declare no conflict of interest.

References

1. Dipika, J.; Malviya, A. Composites for wastewater purification: A review. *Chemosphere* **2020**, *246*, 125788. [[CrossRef](#)]
2. Cana, O.T.; Kobayaa, M.; Demirbasb, E.; Bayramoglu, M. Treatment of the textile wastewater by combined electrocoagulation. *Chemosphere* **2006**, *62*, 181–187. [[CrossRef](#)] [[PubMed](#)]
3. Tak-Hyun, K.; Chulhwan, P.; Eung-Bai, S.; Sangyong, K. Decolorization of disperse and reactive dyes by continuous electrocoagulation process. *Desalination* **2002**, *150*, 165–175. [[CrossRef](#)]
4. Ait Himi, M.; El Ghachtouli, S.; Amarray, A.; Zaroual, Z.; Bonnaillie, P.; Azzi, M. Nanostructured manganese oxide as an efficient eco-friendly catalyst for removing azo dye Calcon from water. *Mater. Today* **2021**, *37*, 3905–3912. [[CrossRef](#)]
5. Islam, M.A.; Ali, I.; Karim, S.A.; Firoz, M.S.H.; Chowdhury, A.N.; Morton, D.W.; Angove, M.J. Angove. Removal of dye from polluted water using novel nano manganese oxide-based materials. *J. Water Process Eng.* **2019**, *32*, 100911. [[CrossRef](#)]
6. Zhao, X.; Lv, L.; Pan, B.; Zhang, W.; Zhang, S.; Zhang, Q. Polymer-supported nanocomposites for environmental application: A review. *Chem. Eng. J.* **2011**, *170*, 381–394. [[CrossRef](#)]
7. Wei, J.; Li, K.; Yu, H.; Yin, H.; Cohen Stuart, M.A.; Wang, J.; Zhou, S. Controlled Synthesis of Manganese Oxide Nanoparticles Encaged in Hollow Mesoporous Silica Nanoreactors and Their Enhanced Dye Degradation Activity. *J. Am. Chem. Soc.* **2020**, *5*, 6852–6861. [[CrossRef](#)] [[PubMed](#)]
8. Su, Q.; Pan, B.; Pan, B.; Zhang, Q.; Zhang, W.; Lv, L.; Wang, X.; Wu, J.; Zhang, Q. Fabrication of polymer-supported nanosized hydrous manganese dioxide (HMO) for enhanced lead removal from waters. *Sci. Total. Environ.* **2009**, *407*, 5471–5477. [[CrossRef](#)]
9. Nasrollahzadeh, M.; Shafiei, N.; Nezafat, Z.; Bidgoli, N.S.S.; Soleimani, F. Recent progresses in the application of cellulose, starch, alginate, gum, pectin, chitin and chitosan based (nano)catalysts in sustainable and selective oxidation reactions: A review. *Carbohydr. Polym.* **2020**, *241*, 116353. [[CrossRef](#)]
10. Swatloski, R.P.; Spear, S.K.; Holbrey, J.D.; Rogers, R.D. Dissolution of Cellulose with Ionic Liquids. *J. Am. Chem. Soc.* **2002**, *124*, 4974–4975. [[CrossRef](#)]
11. Liu, Z.; Wang, H.; Li, Z.; Lu, X.; Zhang, X.; Zhang, S.; Zhou, K. Characterization of the regenerated cellulose films in ionic liquids and rheological properties of the solutions. *Mater. Chem. Phys.* **2011**, *128*, 220–227. [[CrossRef](#)]

12. Peng, R.; Zhang, H.; Gui, L.; Wu, Z.; Yu, P.; Luo, Y. Facile Synthesis of MnO₂@Cellulose Composite Film. *Environ. Eng. Sci.* **2019**, *36*, 583–588. [[CrossRef](#)]
13. Oliveira, L.V.F.; Bennici, S.; Josien, L.; Limousy, L.; Bizeto, M.A.; Camilo, F.F. Free-standing cellulose film containing manganese dioxide nanoparticles and its use in discoloration of indigo carmine dye. *Carbohydr. Polym.* **2020**, *230*, 115621. [[CrossRef](#)]
14. Sun, H.; Xu, K.; Huang, M.; Shang, Y.; She, P.; Yin, S.; Liu, Z. One-pot synthesis of ultrathin manganese dioxide nanosheets and their efficient oxidative degradation of Rhodamine B. *Appl. Surf. Sci.* **2015**, *357*, 69–73. [[CrossRef](#)]
15. Sun, H.; Shang, Y.; Xu, K.; Tang, Y.; Li, J.; Liu, Z. MnO₂ aerogels for highly efficient oxidative degradation of Rhodamine B. *RSC Adv.* **2017**, *7*, 30283–30288. [[CrossRef](#)]
16. Zhang, Y.; Zheng, T.X.; Hu, Y.B.; Guo, X.L.; Peng, H.H.; Zhang, Y.X.; Feng, L.; Zheng, H.L. Delta manganese dioxide nanosheets decorated magnesium wire for the degradation of methyl orange. *J. Colloid. Interf. Sc.* **2017**, *490*, 226–232. [[CrossRef](#)] [[PubMed](#)]
17. Islam, A.; Morton, D.W.; Johnson, B.B.; Mainali, B.; Angove, M.J. Manganese oxides and their application to metal ion and contaminant removal from wastewater. *J. Water Process. Eng.* **2018**, *26*, 264–280. [[CrossRef](#)]
18. Brock, R.M.; Sanabria, M.; Suib, S.L.; Urban, V.; Thiyagarajan, P.; Potter, D.I. Particle Size Control and Self-Assembly Processes in Novel Colloids of Nanocrystalline Manganese Oxide. *J. Phys. Chem. B* **1999**, *103*, 7416–7428. [[CrossRef](#)]
19. Zhou, S.; Ray, A.K. Kinetic Studies for Photocatalytic Degradation of Eosin B on a Thin Film of Titanium Dioxide. *Ind. Eng. Chem. Res.* **2003**, *42*, 6020–6033. [[CrossRef](#)]
20. Morimoto, T.; Kattika, S. Isoelectric point of manganese oxide. *Bull. Chem. Soc. Jpn.* **1974**, *47*, 1586–1588. [[CrossRef](#)]
21. Gray, M.J.; Malati, M.A.; Rophael, M.W. The point of zero charge of manganese dioxides. *J. Electroanal. Chem.* **1978**, *89*, 135–140. [[CrossRef](#)]
22. Biesinger, M.C.; Payne, B.P.; Grosvenor, A.P.; Lau, L.W.M.; Gerson, A.R.; Smart, R.S.C. Resolving surface chemical states in XPS analysis of first row transition metals, oxides and hydroxides: Cr, Mn, Fe, Co and Ni. *Appl. Surf. Sci.* **2011**, *257*, 2717–2730. [[CrossRef](#)]